Soils and Foundations 2014;54(2):116–125

The Japanese Geotechnical Society

Soils and Foundations

www.sciencedirect.com
journal homepage: www.elsevier.com/locate/sandf

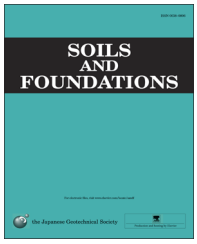

Thermal properties of boring core samples from the Kanto area, Japan: Development of predictive models for thermal conductivity and diffusivity

Takeshi Saito[a,g,*], Shoichiro Hamamoto[b,g], Ei Ei Mon[a,g], Takato Takemura[c,g], Hirotaka Saito[d,g], Toshiko Komatsu[a,e,g], Per Moldrup[f,g]

[a]Graduate School of Science and Engineering, Saitama University, 255 Shimo-Okubo, Sakura-ku, Saitama, Japan
[b]Graduate School of Agricultural and Life Sciences, The University of Tokyo, Bunkyo-ku, Tokyo, Japan
[c]Department of Geosystem Sciences, College of Humanities and Sciences, Nihon University, Setagaya-ku, Tokyo, Japan
[d]Institute of Agriculture, Tokyo University of Agriculture and Technology, Fuchu City, Tokyo, Japan
[e]Institute for Environmental Science and Technology, Saitama University, Sakura-ku, Saitama, Japan
[f]Department of Civil Engineering, Aalborg University, Aalborg, Denmark
[g]Core Research for Evolutionary Science and Technology, Japan Science and Technology Agency, Kawaguchi City, Saitama, Japan

Received 4 December 2012; received in revised form 9 September 2013; accepted 2 October 2013
Available online 26 March 2014

Abstract

The subsurface of the Earth is facing evermore thermal impact due to global warming, urban heat islands, and the widespread use of ground source heat pump (GSHP) systems. This potentially causes changes in its physical, mechanical, microbiological, and chemical properties, and in the subsurface water quality. To predict and evaluate this thermal impact (or thermal pollution), a better understanding and improved models for the thermal properties governing heat transport in subsurface sediments are needed. Also, data acquisition in high spatial resolution for the thermal properties and basic physical properties of the subsurface sediments are essential. In this study, the main thermal properties (the thermal conductivity, heat capacity, and thermal diffusivity) together with the basic physical properties (the soil texture, water content, and dry bulk density) were measured on boring core samples representing depths from 0 to 50 or 80 m, at three study sites in the Kanto area of Japan. Based on the measured data, models for thermal conductivity as functions of gravimetric water content, dry bulk density, and volumetric sand content were developed. The new models performed markedly better than presently available models from the literature and, in combination with a modified de Vries type model for heat capacity, the resulting model for thermal diffusivity was capable of describing the measured data well. The usefulness of the newly developed models were validated and illustrated by using data from a two-day thermal response test (TRT) performed at one of the three study sites. The new predictive models for the thermal properties used in a numerical heat transport simulation accurately predicted subsurface (5–50 m) temperature changes during the TRT.

Keywords: Geothermal properties; Thermal conductivity; Thermal diffusivity; Predictive models; Geophysical properties; Subsurface temperature change; Thermal response test (TRT)

1. Introduction

While global warming is now widely recognized as one of the major environmental problems facing our planet, the possible analog subsurface warming effect has not received much attention (Taniguchi et al., 2009). It has been shown that subsurface warming is strongly associated with surface warming including the global warming effects (Harris and Chapman,

*Corresponding author at: Graduate School of Science and Engineering, Saitama University, 255 Shimo-Okubo, Sakura-ku, Saitama, Japan.
Tel./fax: +81 48 858 9146.
E-mail address: saitou@mail.saitama-u.ac.jp (T. Saito).
Peer review under responsibility of The Japanese Geotechnical Society.

Production and hosting by Elsevier

http://dx.doi.org/10.1016/j.sandf.2014.02.004

1997; Pollack et al., 1998; Huang et al., 2000). Studies have reported a small but significant temperature rise in subsurface environment up to 100–200 m depths below many larger cities in the world (Perrier et al., 2005; Taniguchi et al., 2007; Kooi, 2008). Large underground facilities such as subways and shopping malls along with the rapidly expanding urbanization creating "Urban Heat Islands" (Allen et al., 2003; Taniguchi et al., 2003) may in part explain these changes in subsurface temperatures.

Recently, ground source heat pump (GSHP) systems have become increasingly popular for obtaining energy for heating and cooling with minimal climate impact (Spitler, 2005; Banks, 2008; Dinçer and Rosen, 2011). The GSHP system exchanges heat with the subsurface environment for indoor heating (winter situation) and cooling (summer situation) (Florides and Kalogirou, 2007; Gao et al., 2009). A temperature rise of up to approximately 10 °C in the subsurface monitoring wells in the vicinity of GSHP systems has been observed in several countries (Sowers et al., 2006; Bonte et al., 2011).

Subsurface temperature changes may cause changes in physical, mechanical, microbiological, and chemical properties, as well as in the subsurface water quality. To predict and evaluate the thermal impact (or thermal pollution), a better understanding and improved models for the thermal properties governing heat transport in subsurface sediments are needed. Also, data acquisition in high spatial resolution for both the thermal properties and the basic physical properties (i.e., the soil texture, water content, and dry bulk density) of the subsurface sediment samples are essential since little data is presently available.

The heat transport process in porous media is governed by thermal properties, i.e. thermal conductivity, heat capacity, and thermal diffusivity. Previous studies have investigated the relationships between thermal conductivity and basic physical properties including mineral composition, dry bulk density, and water content, to develop predictive models (de Vries, 1963; Johansen, 1975, Kasubuchi, 1984; Côté and Konard, 2005; Lu et al., 2007). The widely used prediction models currently available for thermal conductivity require several input parameters, each with a marked measurement uncertainty, cost, and time. There is, however, an increasing need for accurate and realistic heat transport models with minimum input parameters requirement for thermal effect and risk assessment calculations, for example in regard to designing GSHP systems with a minimal effect on the subsurface environment and groundwater quality.

The objectives of this study are therefore as follows: (i) to measure the main thermal properties (the thermal conductivity, heat capacity, and thermal diffusivity) as well as the basic physical properties (the soil texture, water content, and dry bulk density) on boring core samples (0 to 50 or 80 m) from three study sites in the Kanto area of Japan, (ii) based on the measured data to develop accurate, low-parameter predictive models for thermal properties of differently-textured water-saturated samples, and (iii) to validate the models and illustrate their possible use by predicting subsurface (5–50 m) temperature changes during a full-scale, short-term thermal response test (TRT) at one of the three study sites.

2. Materials and methods

2.1. Description of sites

The study sites are located at three universities, Saitama University: SU (Saitama city, Saitama; 35°51′44.146″N, 139°36′34.034″E), Nihon University: NU (Setagaya-ku, Tokyo; 35°39′49.385″N, 139°38′4.752″E), and Tokyo University of Agriculture and Technology: TUAT (Fuchu city, Tokyo; 35°41′1.37″N, 139°28′58.44″E), all in the Kanto area of Japan (Fig. 1a). The boring core samples were obtained from all three sites, and the lengths of those samples at SU, NU and TUAT were 50 m, 80 m and 50 m, respectively. For the NU site, the core samples were taken from two boreholes approximately 1 m apart. The groundwater tables are around 1–2 m, 2–4 m, and 10–12 m below the surface at SU, NU, TUAT, respectively.

2.2. Thermal and physical properties measurements

The main thermal and basic physical properties of the core samples were measured by the following procedures. Dry bulk density and wet bulk density were determined on intact subcores (retrieved from the larger columns by a cores sampler) of 7.85 cm^3 (2.0 cm in diameter and 2.5 cm in height). Subsequently, thermal conductivity and heat capacity were measured by a portable KD2 Pro thermal probe (Decagon Devices, Inc.), based on the transient line heat source measurement principle. The probe used has two needles functioning as the heater and temperature sensor, respectively. The temperature sensor monitors the temperature versus time relationship necessary for calculating thermal conductivity and heat capacity (Decagon Devices, 2012). Thermal diffusivity was calculated from the measured thermal conductivity and heat capacity. After the determination of the thermal properties and bulk densities, the gravimetric water content, particle density (AccuPyc 1330 Pycnometer, Micromeritics Instrument Corporation), and particle size distribution (Laser Diffraction Particle Size Analyzer SALD-3100, Shimadzu Corporation) were measured. Following the definition of The Japanese Geotechnical Society, the clay, silt, and sand fractions were defined as <5 μm, 5–75 μm, and 75–2000 μm, respectively. The total porosity was calculated from the dry bulk density and the particle density.

For the subsurface temperature simulation described below, some values of the basic physical properties were obtained by interpolation between the data for the two nearest depths. This was assumed to be accurate since the data were measured with high spatial resolution (typically 1 m between measurements).

2.3. Thermal response test

At the SU site (Fig. 1b), an in-situ thermal response test (TRT) was performed for two days to estimate the effective thermal conductivity. We note that this will include thermal effects by groundwater flow along the whole length of a U-tube functioning as a heat exchanger. The heat exchanger (a double U-tube) was installed in the borehole at 50 m depth and silica sand was used as backfill material around the U-tube. Resistance-type temperature

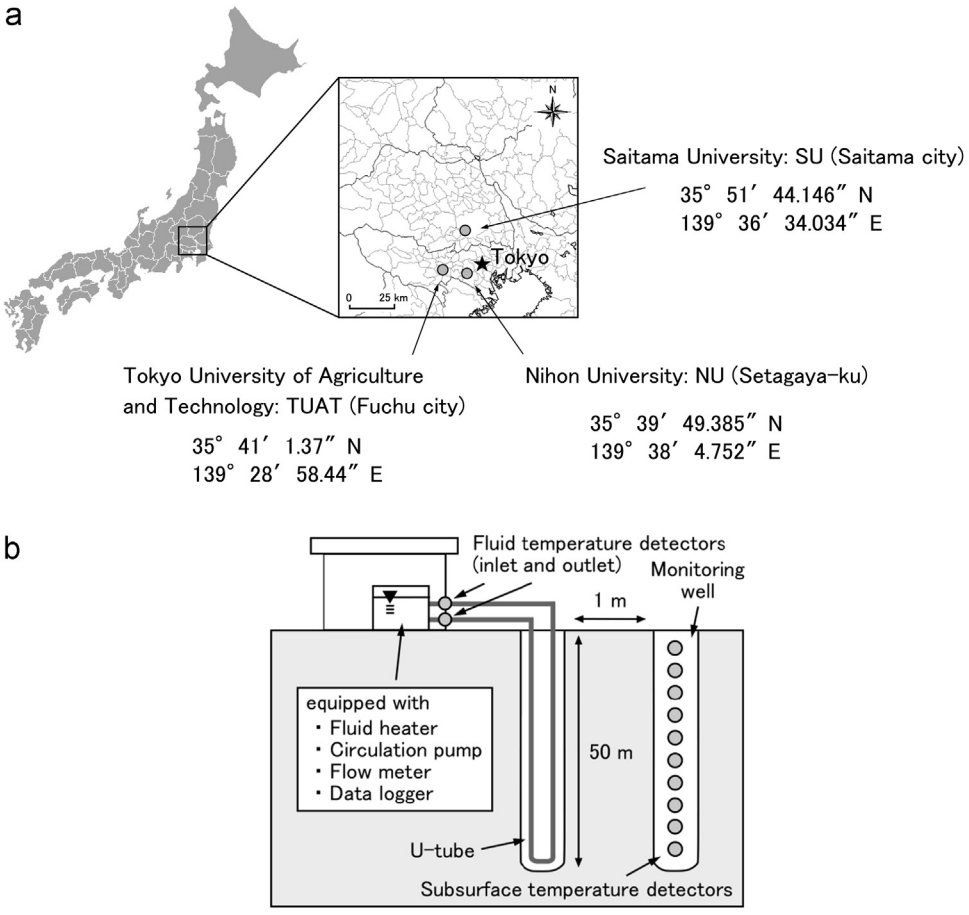

Fig. 1. (a) Location map of study sites (three universities) in the Kanto area of Japan. (b) Schematic diagram for the in-situ thermal response test (TRT) set-up at the SU site.

detectors (R36, Nihondensoku Co., Ltd.) were placed at 10 depths (5.16 m, 10.16 m, 17.14 m, 23.16 m, 27.16 m, 31.16 m, 36.16 m, 39.61 m, 44.16 m and 49.16 m below surface) with 1 m distance from the U-tube, and the subsurface temperature was continuously recorded by a data logger (LR8400, Hioki E. E. Corporation). A fluid (water) heated with a constant energy source (2.5 kW) was circulated through the closed loop, and its temperature was measured at the inlet and outlet of the U-tube. Data were evaluated by the Kelvin's line source theory, which is often used as an analytical technique for TRT results (Signorelli et al., 2007; Yang et al., 2010). Hereby, the effective thermal conductivity λ_e ($W\,m^{-1}\,K^{-1}$) was estimated from the slope m (K) by plotting the average fluid temperature between the inlet and outlet of the U-tube for Y-axis versus the natural logarithm of time (days) (Lee et al., 2012; Wagner et al., 2012), following:

$$\lambda_e = \frac{q}{4\pi m} \tag{1}$$

where q is the heat injection rate per unit length of a heat exchanger ($W\,m^{-1}$).

2.4. Subsurface temperature simulation

The changes in subsurface (5–50 m) temperature profile during the TRT at the SU site were numerically simulated to validate and illustrate the usefulness of new predictive models for the thermal properties. In the cylindrical coordinate system, the governing equation for heat transport can be written as

$$\frac{\partial T}{\partial t} = \frac{\lambda}{C}\left[\frac{\partial^2 T}{\partial r^2} + \frac{1}{r}\frac{\partial T}{\partial r} + \frac{\partial^2 T}{\partial z^2}\right] \tag{2}$$

where T is the temperature (K), λ is thermal conductivity ($W\,m^{-1}\,K^{-1}$), C is heat capacity ($MJ\,m^{-3}\,K^{-1}$), t is time (s), r is radius in the horizontal direction (m), and z is depth (m). In this simulation, only heat conduction process due to the temperature gradient is considered as a heat transport mechanism since in-situ measurements of the groundwater flow at the SU site demonstrated that the flow velocity is very low (less than $3.0\times10^{-5}\,cm\,s^{-1}$), and advective heat transport along with the groundwater flow therefore would be negligible during a two-day TRT. Eq. (2) was numerically solved by using COMSOL Multiphysics 3.5a (COMSOL) with a finite element method (described later in detail).

3. Model descriptions

3.1. Available models for the thermal properties

de Vries (1963) proposed a widely used model for estimating thermal conductivity λ ($W\,m^{-1}\,K^{-1}$) by considering the

volumetric fractions of each component (i.e., water, sand, silt, clay, and air), weighting factors associated with the thermal conductivities for each component, and taking the geometric shape of the solid particles into account. This model can be expressed in a general form as

$$\lambda = \frac{\sum_{i=1}^{N} k_i V_i \lambda_i}{\sum_{i=1}^{N} k_i V_i} \tag{3a}$$

where V_i is the volumetric fraction ($m^3\ m^{-3}$), and k_i is the weighting factor determined by the thermal conductivity (λ_i). The subscript (i) means a component of the measured sample (i.e., water, sand, silt, clay, or air). In case of water as the liquid phase, k_i is taken as 1.0. For the mineral components, k_i can be calculated from the following relationship:

$$k_i = \frac{1}{3} \sum_{j=a,b,c} \left[1 + \left(\frac{\lambda_i}{\lambda_0} - 1 \right) g_{ij} \right]^{-1} \tag{3b}$$

where g_{ij} is the geometric shape factor for a given solid phase i (i.e., sand, silt, or clay), and the subscript (j) represents the ratios of the axes a, b, and c for the solid particle, satisfying $g_{ia}+g_{ib}+g_{ic}=1$. The value λ_0 is the thermal conductivity of air under fully dry conditions, while the thermal conductivity of water is used as the λ_0 value under water-saturated conditions. In this study, two solids phases were considered, the coarser particles represented by sand and the finer particles represented by silt and clay (hereafter labeled silt–clay). The thermal conductivities of sand solids (λ_{sand}), silt–clay solids ($\lambda_{silt-clay}$) and water (λ_w) were taken as 3.0, 2.93, and 0.6 W $m^{-1}\ K^{-1}$ (de Vries, 1963; Hwang et al., 2006), respectively. The geometric shape factors were set at g_a=0.125, g_b=0.125, and g_c=0.75 for sand, and g_a=1, g_b=0, and g_c=0 for silt–clay, assuming ellipsoid particle shape for sand, and lamellae particle shape for silt–clay, respectively (de Vries, 1963).

Johansen (1975) developed a thermal conductivity prediction model for water saturated conditions, based on the thermal conductivities of water (λ_w) and solid particles (λ_s). The thermal conductivity under water-saturated condition λ_{sat} is (Johansen, 1975)

$$\lambda_{sat} = \lambda_s^{1-n} \lambda_w^n \tag{4a}$$

where n is the total porosity of the sample and a value of 0.6 W $m^{-1}\ K^{-1}$ was used for λ_w. In this model, the λ_s value is determined from the volumetric quartz content (q), and the thermal conductivities of quartz (λ_{quartz}=7.7 W $m^{-1}\ K^{-1}$) and other minerals (λ_0), using:

$$\lambda_s = \lambda_{quartz}^{q} \lambda_0^{1-q} \tag{4b}$$

Johansen (1975) suggested λ_0 of 2.0 (W $m^{-1}\ K^{-1}$) for $q > 0.2$, and 3.0 for $q \le 0.2$. In this study, λ_s was simply taken as 3.0, since this is very close to the values of the thermal conductivities for both sand (λ_{sand}=3.0) and silt–clay ($\lambda_{silt-clay}$=2.93).

A general mixing model, defined by assuming independent parallel layer of each phase (i) (i.e., water, solid, and air), can be written as follows:

$$\lambda = \sum_{i=1}^{N} V_i \lambda_i \tag{5a}$$

where V_i is the volumetric fraction of each phase ($m^3\ m^{-3}$). The thermal conductivity of the solid phase (λ_s) can be estimated from a weighted geometric mean (Eq. (5b)) of the thermal conductivities of each solids fraction (Kasubuchi, 1984):

$$\lambda_s = \lambda_{sa}^{V_{sa}} \lambda_{sb}^{V_{sb}} \tag{5b}$$

where λ_{sa} and λ_{sb} are the thermal conductivities of the components a and b, respectively. The V_{sa} and V_{sb} are the volumetric fractions of each component, satisfying $V_{sa}+V_{sb}=1$. When applying this model in the present study, the thermal conductivities of the sand ($\lambda_a=\lambda_{sand}$=3.0 W $m^{-1}\ K^{-1}$), silt–clay ($\lambda_b=\lambda_{silt-clay}$=2.93), and water ($\lambda_w$=0.6) were used.

de Vries (1963) proposed a predictive heat capacity model, which is one of the most frequently use relations in geothermal studies:

$$C = 0.46 V_s + 0.60 V_o + \theta \tag{6a}$$

where C is the heat capacity (cal $cm^{-3}\ K^{-1}$), here calculated from the volumetric fractions ($m^3\ m^{-3}$) of solid particle (V_s), organic matter (V_o), and water (θ). Eq. (6a) is the original equation by de Vries (1963), and it was used in this study by converting the original unit of C (cal $cm^{-3}\ K^{-1}$) to (MJ $m^{-3}\ K^{-1}$). Furthermore, assuming that there is no organic matter (V_o=0) and the measured samples are under water-saturated condition, the following equation for heat capacity can be derived from Eq. (6a):

$$C = 4.20\theta + 1.93(1-\theta) \tag{6b}$$

where C is in units of (MJ $m^{-3}\ K^{-1}$).

3.2. Sensitivity analyses of the models

In order to evaluate the performance of the considered prediction models for thermal conductivity, two different statistical indices, root mean square error (RMSE) and bias (Lu et al., 2007; Hamamoto et al., 2011; Dissanayaka et al., 2012) were used. The RMSE was applied to evaluate the overall performance or best-fit of the models:

$$\mathrm{RMSE} = \sqrt{\frac{1}{N} \sum_{i=1}^{N} (\lambda_{mi} - \lambda_{pi})^2} \tag{7}$$

where N is the number of measurements. The values λ_{mi} and λ_{pi} are the measured and predicted thermal conductivities, respectively.

The bias was used to evaluate overestimation or underestimation of the models as compared to the measured data:

$$\mathrm{bias} = \frac{1}{N} \sum_{i=1}^{N} (\lambda_{mi} - \lambda_{pi}) \tag{8}$$

4. Results and discussion

4.1. Depth profiles of the measured thermal and physical properties

The depth profiles of particle size distribution (%), gravimetric water content (%), dry and wet bulk densities (Mg m^{-3}), total porosity (%), thermal conductivity (W m^{-1} K^{-1}), and heat capacity (MJ m^{-3} K^{-1}) at each site are presented in Fig. 2. At the SU site, the gravimetric water content at approximately 40 m depth was very low due to the existence of sand gravel layer, which has a small water retention capacity. In addition, relatively higher thermal conductivity was observed below depths of 45 m. In the surface layers of the NU and TUAT sites, higher values of gravimetric water content and total porosity, and lower values of dry bulk density and thermal conductivity were observed compared to the deeper part of the profiles at both sites. The reason for this is that the upper surface formations in the Kanto area consist of volcanic ash soils (loamy layers) with a high organic matter content (around 10–22%). At the NU site, sand layers were dominant below 15 m depth, and the values of thermal and physical properties were almost constant with depth. For all sites, the heat capacity was almost constant, with an average value of 3.05 (MJ m^{-3} K^{-1}).

4.2. Development of new models for the thermal properties

The theermal conductivity λ (W m^{-1} K^{-1}), heat capacity C (MJ m^{-3} K^{-1}), and thermal diffusivity α ($\times 10^{-6}$ m^2 s^{-1}) as functions of gravimetric water content ω (%) and dry bulk density ρ_b (Mg m^{-3}) are presented in Fig. 3. The measured λ demonstrated a non-linear decrease with increasing ω (Fig. 3a), because all samples were near water saturation and thus only acted as a two-phase system (water and solids) without air. Therefore, the λ–ω relation could be expressed by a power-law function, assuming that the value of λ at high ω approaches the thermal conductivity of water (0.6 W m^{-1} K^{-1}) (no solids present) and, also, becomes equal to the thermal conductivity of solid particle (3.0 W m^{-1} K^{-1}) at ω of 0 (only solids present). When the power-law function is fitted to the measured data for fully water-saturated samples, the resulting equation is given as

$$\lambda = 2.4\omega^{-0.016\omega} + 0.6 \tag{9}$$

The upper, loamy layer data, which can be considered as unsaturated samples above the groundwater table, at the NU and TUAT sites were excluded for the model development, since these layers had a very high organic matter content as compared with the deeper parts of both sites. Also, the data of the sand gravel layer at the SU site were not included, because the λ value could not be measured (the thermal probe could not be inserted into the samples). Besides Eq. (9) (thick solid line), suggested upper-limit and lower-limit models for λ–ω are also plotted (as thin solid lines) in Fig. 3a.

Data indicated that the λ value was also related non-linearly to ρ_b (Fig. 3b). This non-linear relationship for λ–ρ_b can be derived by inserting the following relationship in Eq. (9):

$$\omega = \frac{255 - 100\rho_b}{2.55\rho_b} \tag{10}$$

In Eq. (10) the solids particle density is assumed to be 2.55 (Mg m^{-3}), corresponding to the average value (2.55 ± 0.17) of all boring core samples, again with the exception of the samples from the unsaturated high-organic loamy layers. Basically, the ω dependent λ model (Eq. (9)) captured the measured data well as compared to ρ_b dependent λ model which slightly underestimated the data probably due to the assumption of constant particle density under the fully water-saturated condition.

For the heat capacity C (MJ m^{-3} K^{-1}), there were no clear relations to either ω or ρ_b (Fig. 3c and d). However, these relations ($C-\omega$ and $C-\rho_b$) could be determined by the modified de Vries type model (Eq. (6b)), by applying:

$$\theta = \frac{2.55\omega}{100 + 2.55\omega} \tag{11}$$

$$\theta = \frac{255 - 100\rho_b}{255} \tag{12}$$

where θ is the volumetric water content (m^3 m^{-3}), and the solids particle density is again assumed equal to 2.55 (Mg m^{-3}) in both equations. The solid lines in Fig. 3c and d show the proposed predictive models for C well described the range of the obtained heat capacity.

The trends of the thermal diffusivity α ($\times 10^{-6}$ m^2 s^{-1}) plotted against ω and ρ_b were similar to those of the λ relations (Fig. 3e and f). The thermal diffusivity, α, is obtained by dividing the thermal conductivity, λ (Eq. (9)), by the heat capacity, C. First, combining Eqs. (6b) and (11) to obtain C as a function of ω, $C(\omega)$, Eq. (13) gives α as a function of ω:

$$\alpha = \frac{\lambda}{C(\omega)} = \frac{(0.6 + 2.4\omega^{-0.016\omega})}{[1.93 + 5.79\omega/(100 + 2.55\omega)]} \tag{13}$$

Second, combining Eqs. (6b) and (12) to obtain $C(\rho_b)$, Eq. (14) can be used to calculate α as a function of ρ_b:

$$\alpha = \frac{\lambda}{C(\rho_b)} = \frac{0.6 + 2.4\omega(\rho_b)^{-0.016\omega(\rho_b)}}{4.2 - 0.89\rho_b} \tag{14}$$

where ω as a function of ρ_b, $\omega(\rho_b)$, is given by Eq. (10). The relations (Eqs. (13) and (14)) are shown by thick solid lines in Fig. 3e and f, respectively. As expected from Fig. 3a and c, the proposed ω-dependent α model accurately predicted the measured α. It is noted that almost as good predictions were obtained when a constant, average heat capacity ($C = 3.05$ MJ m^{-3} K^{-1}) was used as the denominator in Eqs. (13) and (14). These simplified models are shown as thin solid lines in Fig. 3e and f.

Fig. 4 presents the measured λ (W m^{-1} K^{-1}) as a function of volumetric sand content V_{sand} (%), with the regression line and the 95% confidence interval. The best fit model yielded:

$$\lambda = 0.006V_{sand} + 0.875 \tag{15}$$

In agreement with Eq. (15), the measured λ generally increased with increasing V_{sand}. This simple model for thermal conductivity (Eq. (15)) seems especially useful if the soil texture is

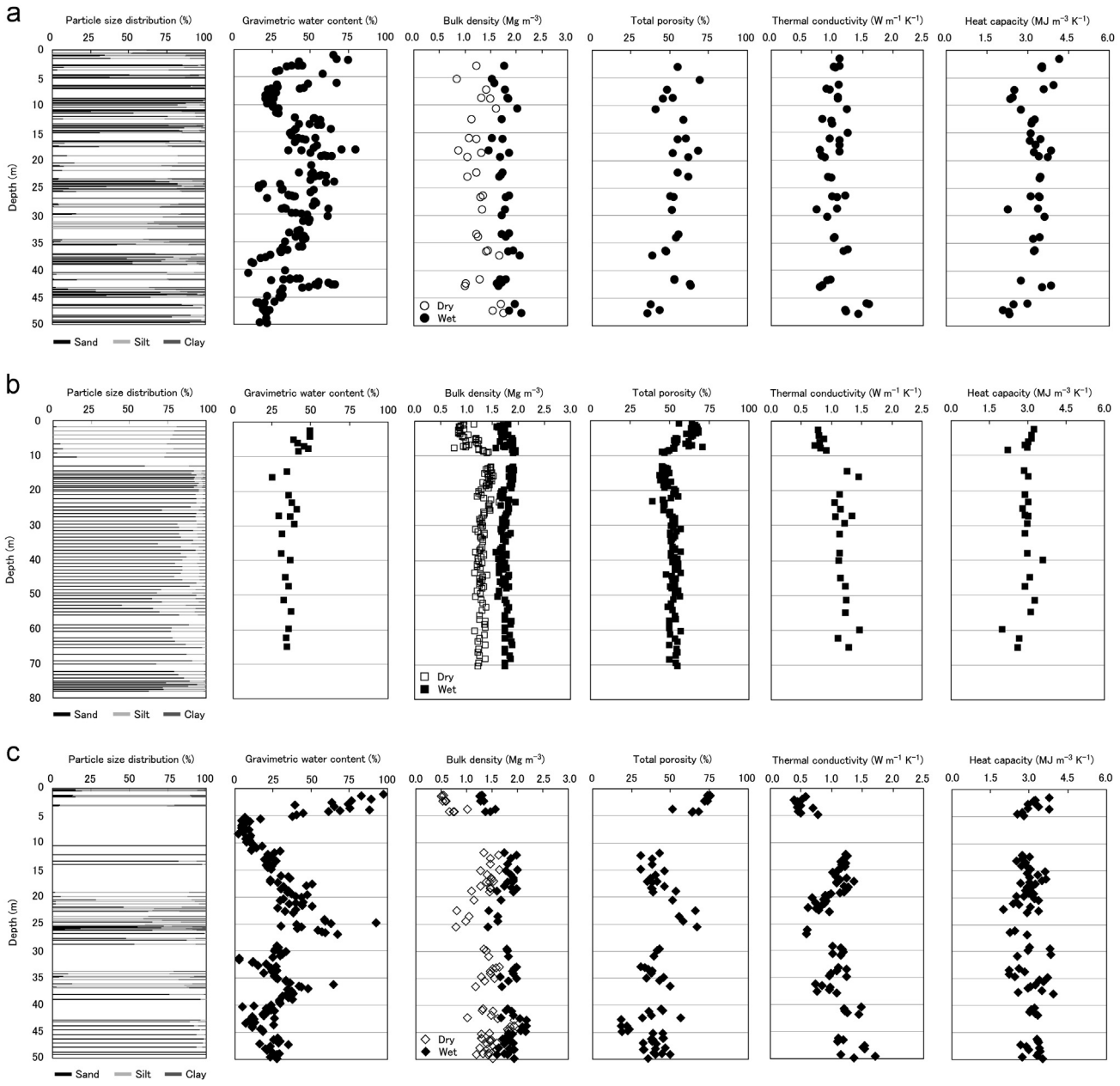

Fig. 2. Depth profiles of measured particle size distribution (%), gravimetric water content (%), dry bulk density and wet bulk density (Mg m^{-3}), total porosity (%), thermal conductivity (W m^{-1} K^{-1}), and heat capacity (MJ m^{-3} K^{-1}) for the boring core samples from (a) SU, (b) NU and (c) TUAT sites. The total porosity was calculated by using average particle density at each site: 2.69±0.08 (SU), 2.57±0.20 (upper loamy layers at NU), 2.66±0.04 (the other layers at NU), 2.07±0.15 (upper loamy layers at TUAT), and 2.36±0.10 (the other layers at TUAT).

known while moisture conditions (water content) are unknown. If both water content and texture are known, it is recommended to use and compare both predictive λ models to obtain a further estimate of prediction uncertainty.

4.3. Model validation and subsurface temperature simulation

Fig. 5 shows the scatter plot of the measured versus predicted λ values (W m^{-1} K^{-1}) by the proposed model as a function of gravimetric water content (Eq. (9)) (Fig. 5a) and by presently available models (Eq. (3)–(5)) (Fig. 5b). The values of RMSE and bias (Eqs. (7) and (8)) are also presented in Fig. 5a and b. The newly developed model performed well, showing less than 30% prediction error for most predicted values, and gave better prediction accuracy than the three presently available models. Among these three comparison models, the Johansen model (Eq. (4)) demonstrated a slightly better performance than the other two models (Eqs. (3) and (5)), most likely because it is developed specifically for the water-saturated condition. However, all three models overestimated the measured data, giving negative values of bias. Perhaps the reason why the three comparison models (Eqs. (3) and (5)) did not perform well is the need for additional input parameters, such as a geometric shape factor and the volumetric quartz content. Because it is difficult

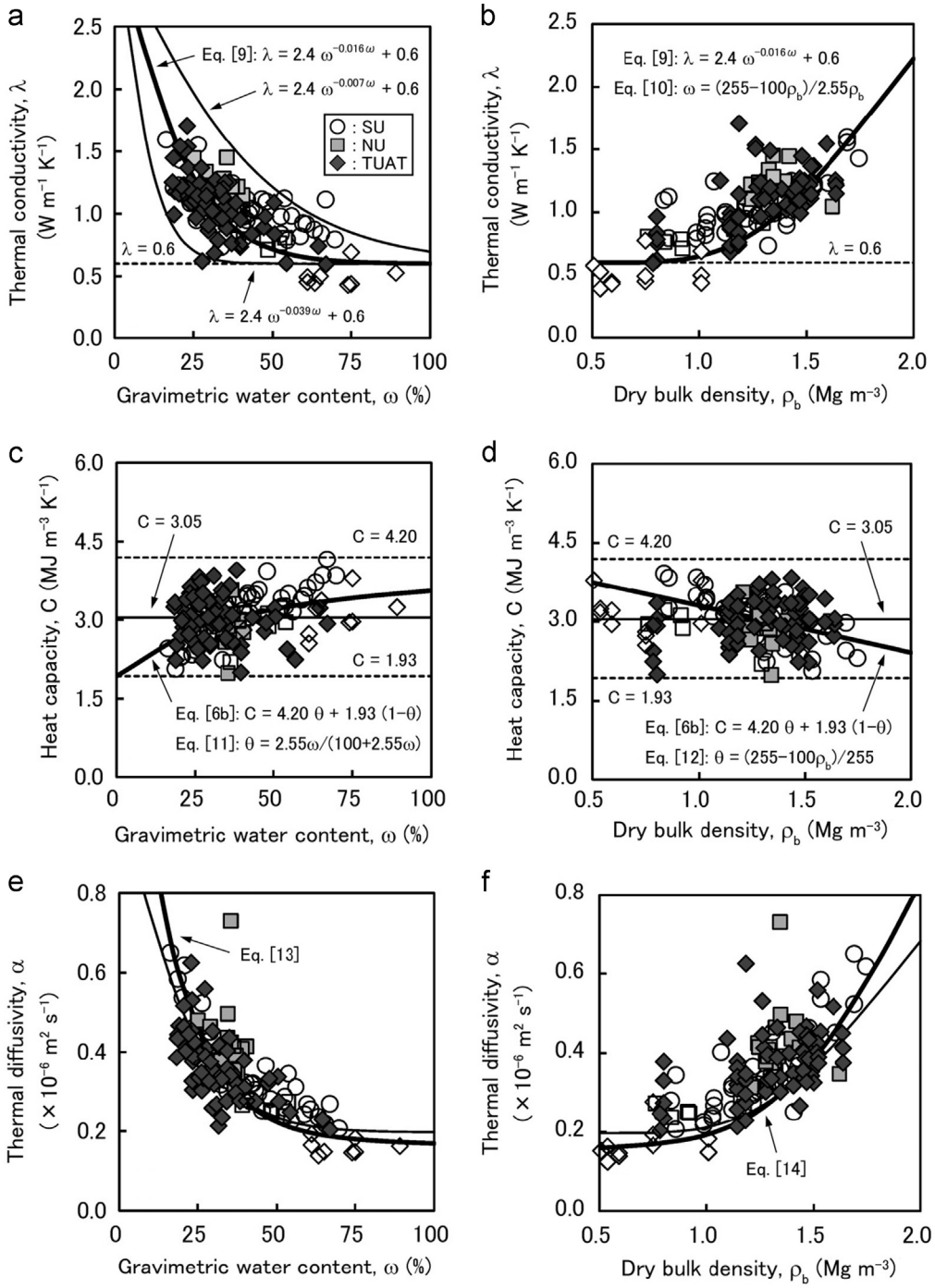

Fig. 3. Thermal conductivity λ (W m^{-1} K^{-1}), heat capacity C (MJ m^{-3} K^{-1}), and thermal diffusivity α ($\times 10^{-6}$ m^2 s^{-1}) as functions of gravimetric water content ω (%) and dry bulk density ρb (Mg m^{-3}) for all measured data at the three sites. The upper loamy layer data at NU and TUAT sites are represented by open symbols.

to determine these parameters, the amount of uncertainty in the model is larger. The proposed predictive model for thermal conductivity as a function of gravimetric water content (Eq. (9)) with less input parameter requirement seems highly useful for predicting thermal conductivity, showing a higher predictive ability for differently-textured sediments within the Kanto area.

Fig. 6a presents the temporal variation of the fluid temperature (°C) at the inlet and outlet of the U-tube for two days during the TRT. The average fluid temperature against the natural logarithm of time (days) and the tangent line to the relation are shown in Fig. 6b. The effective thermal conductivity λ_e (1.71 W m^{-1} K^{-1}) was estimated by inserting the slope of the tangent line, $m=2.63$ (K), and the heat exchange rate, $q=56.35$ (W m^{-1}), into Eq. (1). The hereby obtained λ_e was clearly higher than the non-TRT-affected λ values at the SU site, as measured by the portable analyzer (Fig. 2).

The changes in subsurface temperature profiles were simulated by using (i) measured values of the thermal properties at the SU site (Fig. 2) with interpolation between data using a spline function, (ii) constant thermal conductivity obtained

from the TRT (1.71 W m^{-1} K^{-1}) and the average heat capacity at the SU site (3.17 MJ m^{-3} K^{-1}), and (iii) predicted thermal properties from the newly developed models as a function of the gravimetric water content (Eqs. (9), (6b), and (11)). The gravimetric water content was also interpolated by a spline function, giving model-predicted λ and C depth profiles (Fig. 7a). The model domain of the numerical heat transport is shown in Fig. 7b. A 50 m depth of the U-tube as a heat exchanger and a 10 m radius were set in the domain. The diameter of the borehole for the U-tube was approximately 0.16 m, and the spacing between the U-tube and the ground was filled with silica sand, having λ of 4.0 (W m^{-1} K^{-1}) and C of 3.0 (MJ m^{-3} K^{-1}) (Smits et al., 2010). The silica sand layer was assumed to take up 0.08 m of radius at the location of U-tube (i.e., around the central axis through the U-tube). The thermal insulation and the average air temperature (283.15 K) during the TRT (2 days) were applied as both bottom and lateral boundaries, and a top boundary, respectively. The average fluid temperature at inlet and outlet of the U-tube with time based on the TRT (Fig. 6b), and measured subsurface temperature depth profile before the TRT shown with a black solid line in Fig. 7c, were applied as a central axis boundary and the initial condition of the model domain, respectively. Totally 7100 triangular finite element meshes were produced in the domain, and the numerical simulation was conducted with a time interval of 1 h for two days.

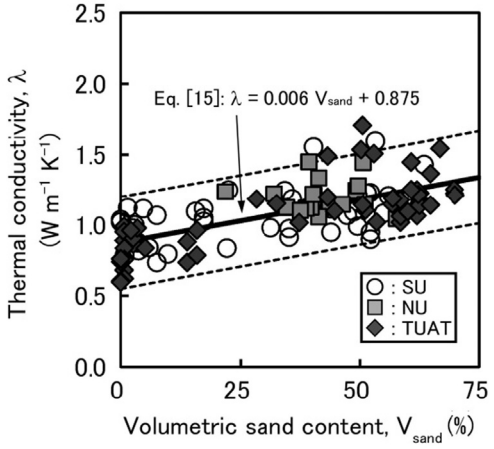

Fig. 4. Measured thermal conductivity λ (W m^{-1} K^{-1}) as a function of volumetric sand content V_{sand} (%), for data excluding the upper loamy layer data at the NU and TUAT sites, with regression line and the 95% confidence interval.

Fig. 7c shows the measured and simulated subsurface temperature profiles at 1 m distance from the U-tube. Only the simulation using the predicted depth profiles of λ and C values (Fig. 7a; scenario (iii) above) is presented in Fig. 7c. The measured data demonstrated that subsurface temperature increased during the TRT, especially at 10 m and 35–50 m depths. Higher λ caused rapid heat transport at those depths (Fig. 7a), giving a relatively larger increase in the subsurface temperature. The prediction by the proposed gravimetric water content (ω) based models for λ and C (Eqs. (9), (6b), and (11)) agreed well with the measured data (RMSE=0.007 and bias=0.049), and could represent heat transport characteristics in different types of geological formations. Using other thermal properties as input parameters (scenarios (i) and (ii) above) yielded similar TRT simulation results (scenario (i): RMSE=0.010 and bias=0.053, and scenario (ii): RMSE=0.010 and bias=0.047). However, the predictions based on the newly developed models for the thermal properties were in slightly better agreement, as also illustrated in Fig. 8 where the accuracy of the numerical model predictions is compared for the three scenarios (i)–(iii) after the end (2 days) of the TRT. The applicability of the proposed models for even larger changes in subsurface temperature will be evaluated in future studies by acquiring temperature data over a long time period.

5. Summary and conclusions

Thermal conductivity, heat capacity, and thermal diffusivity were measured on boring core samples representing depths from 0 to 50 or 80 m at three study sites in the Kanto area of

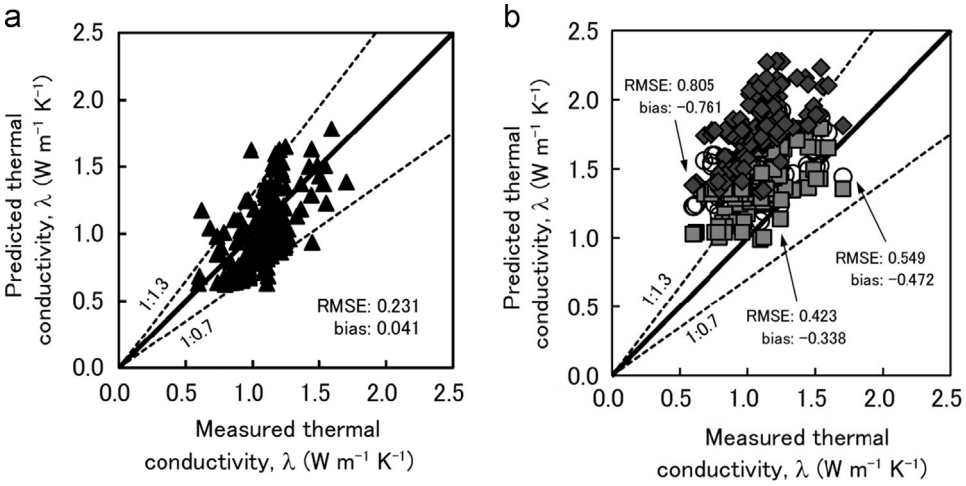

Fig. 5. Scatter plots of measured versus predicted thermal conductivities λ (W m^{-1} K^{-1}) by (a) the proposed model for λ as a function of gravimetric water content ω (%) (Eq. [9]) and by (b) presently available models (Eqs. [3]–[5]) with RMSE and bias values for each model. The legends of circle, square, and diamond shape represent the data by de Vries model, Johansen model, and Mixing model, respectively.

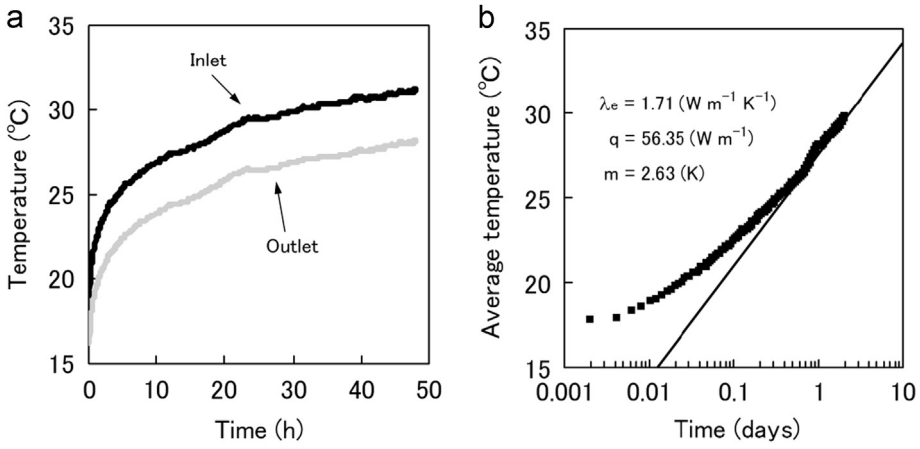

Fig. 6. (a) Temporal variation of the fluid temperature (°C) at the inlet and outlet of the U-tube for a two-day thermal response test (TRT). (b) The average fluid temperature against the natural logarithm of time (days) with the tangent line.

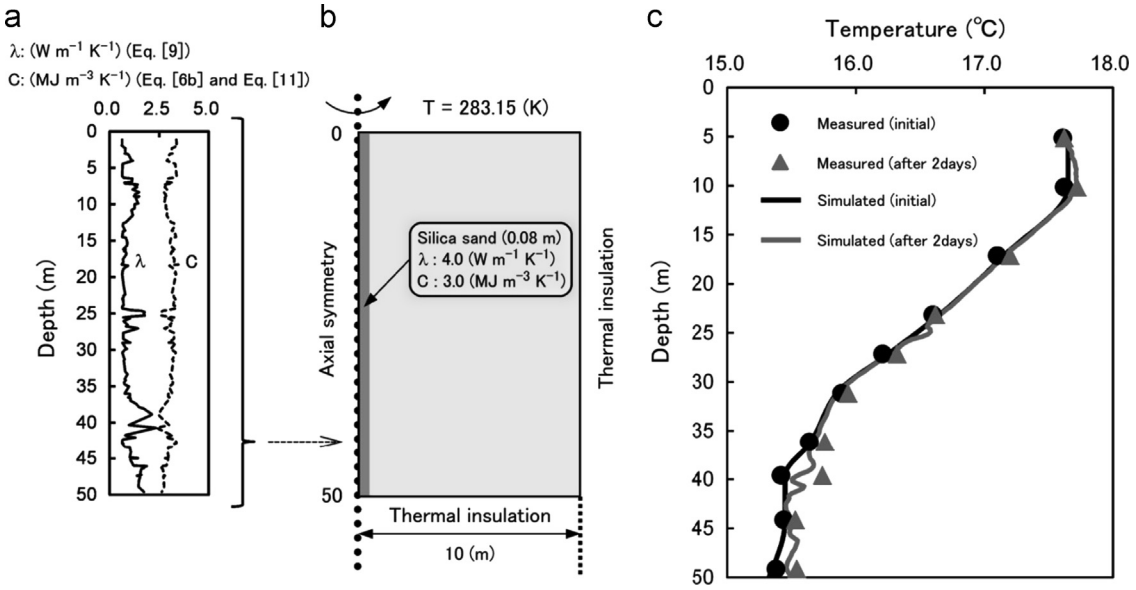

Fig. 7. (a) Depth profiles of predicted thermal properties λ (W m^{-1} K^{-1}) and C (MJ m^{-3} K^{-1}) by the newly developed models, as a function of gravimetric water content ω (%), with data for the latter being interpolated by a spline function. (b) The detailed model domain for the numerical heat transport simulation. (c) The measured and simulated subsurface temperature profiles at 1 m distance from the U-tube during a two-day thermal response test (TRT).

Japan, together with basic physical properties such as soil texture, water content, and dry bulk density. The thermal conductivity showed a non-linear decrease with increasing gravimetric water content and a non-linear increase with increasing dry bulk density, respectively.

From the measured data, predictive models for the thermal conductivity as functions of (i) gravimetric water content, (ii) dry bulk density assuming full water saturation, and (iii) volumetric content of sand were developed. Especially, the water content based model performed well compared with presently available models from literature, showing small RMSE and bias values. In combination with a modified de Vries type model for heat capacity, the resulting model for predicting thermal diffusivity also performed well compared with the measured data.

The usefulness of the new models was preliminary validated by using data from a two day thermal response test (TRT) carried out at one of the study sites. A simple numerical heat transport simulation model in combination with the newly developed predictive models for the thermal properties well predicted the observed temperature changes in the subsurface (5–50 m) during the TRT. These low-parameter models are useful for predicting subsurface temperature changes due to possible thermal impact (or thermal pollution) due to global warming, urban heat islands, and the application of GSHP systems.

In future studies for investigating geothermal system effects on subsurface geosphere, the proposed models for the thermal properties will be further validated by obtaining both thermal and basic physical properties from boring core samples from different locations and types of geological formations in Japan. Also, the development of improved prediction models including, for example, volumetric sand content and mineral

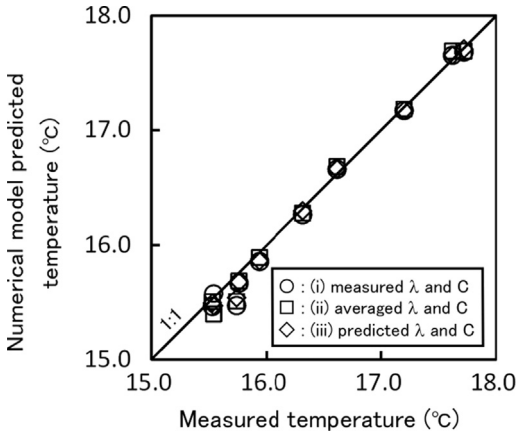

Fig. 8. Scatter-plot comparison of measured versus numerical model predicted temperature after the end of the 2-day thermal response test (TRT), using (i) measured thermal conductivity (λ) and heat capacity (C), (ii) average of λ and C, and (iii) λ and C predicted by the newly developed models (Eq. [9] for λ and Eqs. [6b] and [11] for C).

composition as input parameters will be needed for better understanding the heat transport and thermal impacts ("thermal pollution") in the subsurface environment.

Acknowledgments

This research was supported from Core Research for Evolutionary Science and Technology (CREST) by Japan Science and Technology Agency (JST) and partly supported from Grant-in-Aid for Scientific Research (no. 22860012) by Japan Society for the Promotion of Science (JSPS). The authors are deeply grateful to Dr. Shigeoki Moritani from Tokyo University of Agriculture and Technology (CREST, JST), Dr. Ayako Funabiki from Nihon University (CREST, JST) and Mr. Kenta Tanimoto from Saitama University (CREST, JST) for measuring the thermal and basic physical properties of boring core samples.

References

Allen, A., Milenic, D., Sikora, P., 2003. Shallow gravel aquifers and the urban 'heat island' effect: a source of low enthalpy geothermal energy. Geothermics 32, 569–578.

Banks, D., 2008. An Introduction to Thermogeology: Ground Source Heating and Cooling. Blackwell Publishing Ltd., Oxford, UK.

Bonte, M., Stuyfzand, P.J., Hulsmann, A., van Beelen, P., 2011. Underground thermal energy storage: environmental risks and policy developments in the Netherlands and European Union. Ecol. Soc. 16 (Article 22).

Côté, J., Konard, J.M., 2005. Thermal conductivity of base-course materials. Can. Geotech. J. 42, 61–78.

de Vries, D.A., 1963. Thermal properties of soils. In: van Wijk, W.R. (Ed.), Physics of Plant Environment. North Holland Publishing Company, Amsterdam, Netherlands, pp. 210–235.

Decagon Devices, 2012. KD2 Pro Thermal Properties Analyzer Operator's Manual Version 12. Decagon Devices, Inc., Pullman, USA.

Dinçer, I., Rosen, M.A., 2011. Thermal Energy Storage: Systems and Applications, second ed. John Wiley & Sons Ltd., Chichester, UK.

Dissanayaka, S.H., Hamamoto, S., Kawamoto, K., Komatsu, T., Møldrup, P., 2012. Thermal properties of peaty soils: effects of liquid-phase impedance factor and shrinkage. Vadose Zone J. 11, http://dxdoi.org/10.2136/vzj2011.0092.

Florides, G., Kalogirou, S., 2007. Ground heat exchangers – a review of systems, models and applications. Renew. Energy 32, 2461–2478.

Gao, Q., Li, M., Yu, M., Spitler, J.D., Yan, Y.Y., 2009. Review of development from GSHP to UTES in China and other countries. Renew. Sustain. Energy Rev. 13, 1383–1394.

Hamamoto, S., Møldrup, P., Kawamoto, K., de Jonge, L.W., Schjønning, P., Komatsu, T, 2011. Two-region extended Archie's law model for soil air permeability and gas diffusivity. Soil Sci. Soc. Am. J. 75, 795–806.

Harris, R.N., Chapman, D.S., 1997. Borehole temperatures and a baseline for 20th-century global warming estimates. Science 275, 1618–1621.

Huang, S., Pollack, H.N., Shen, P.Y., 2000. Temperature trends over the past five centuries reconstructed from borehole temperatures. Nature 403, 756–758.

Hwang, S., Ooka, R., Nam, Y., Sekine, K., Shimawaki, Y., 2006. Development of numerical model to predict heat extract and injection rate of ground heat exchanger: part 1 – development of numerical simulation model and simple estimation method for soil properties. J. Soc. Heat. Air-cond. Sanit. Eng. Jpn. 108, 1–10 (in Japanese with English abstract).

Johansen, O., 1975. Thermal Conductivity of Soils (Ph.D. dissertation). University of Trondheim, Norway (CRREL draft translation 637, 1977).

Kasubuchi, T., 1984. Heat conduction model of saturated soil and estimation of thermal conductivity of soil solid phase. Soil Sci. 138, 240–247.

Kooi, H., 2008. Spatial variability in subsurface warming over the last three decades; insight from repeated borehole temperature measurements in the Netherland. Earth Planet. Sci. Lett. 270, 86–94.

Lee, C., Park, M., Nguyen, T.B., Sohn, B., Choi, J.M., Choi, H., 2012. Performance evaluation of closed-loop vertical ground heat exchangers by conducting in-situ thermal response tests. Renew. Energy 42, 77–83.

Lu, S., Ren, T., Gong, Y., Horton, R., 2007. An improved model for predicting soil thermal conductivity from water content at room temperature. Soil Sci. Soc. Am. J. 71, 8–14.

Perrier, F., Le Mouel, J.L., Poirier, J.P., Shnirman, M.G., 2005. Long-term climate change and surface versus underground temperature measurement in Paris. Int. J. Climatol. 25, 1619–1631.

Pollack, H.N., Huang, S., Shen, P.Y., 1998. Climate change record in subsurface temperatures: a global perspective. Science 282, 279–281.

Signorelli, S., Bassetti, S., Pahud, D., Kohl, T., 2007. Numerical evaluation of thermal response tests. Geothermics 36, 141–166.

Smits, K.M., Sakaki, T., Limsuwat, A., lllangasekare, T.H., 2010. Thermal conductivity of sands under varying moisture and porosity in drainage-wetting cycles. Vadose Zone J. 9, 172–180.

Sowers, L., York, K.P., Stiles, L., 2006. Impact of thermal buildup on groundwater chemistry and aquifer microbes. In: Proceedings of the Tenth International Conference on Thermal Energy Storage (ECOSTOCK 2006 Conference). Galloway, USA. 7p.

Spitler, J.D., 2005. Ground-source heat pump system research-past, present, and future. HVAC&R Res. 11, 165–167.

Taniguchi, M., Shimada, J., Uemura, T., 2003. Transient effects of surface temperature and groundwater flow on subsurface temperature in Kumamoto Plain, Japan. Phys. Chem. Earth A/B/C 28, 477–486.

Taniguchi, M., Uemura, T., Jago-on, K., 2007. Combined effects of urbanization and global warming on subsurface temperature in four Asian cities. Vadose Zone J. 6, 591–596.

Taniguchi, M., Shimada, J., Fukuda, Y., Yamano, M., Onodera, S., Kaneko, S., Yoshikoshi, A., 2009. Anthropogenic effects on the subsurface thermal and groundwater environments in Osaka, Japan and Bangkok, Thailand. Sci. Total Environ. 407, 3153–3164.

Wagner, V., Bayer, P., Kübert, M., Blum, P., 2012. Numerical sensitivity study of thermal response tests. Renew. Energy 41, 245–253.

Yang, H., Cui, P., Fang, Z., 2010. Vertical-borehole ground-coupled heat pumps: a review of models and systems. Appl. Energy 87, 16–27.